Supplementary Information (SI) for Journal of Materials Chemistry A.

Electronic Supplementary Information

Development of Single Crystalline Al-doped ZnS Nanodiscs as Efficient Photocatalysts for H_2 Evolution Reaction

Rohit R. Koli[a], *I-Hua Tsai*[a], *Yu-Bin Huang*[b], *Chia-Hsin Wang*[b], *Bo-Hong Liu*[b], *Raghunath Putikam*[a], *M. C. Lin*[a], *Eric Wei-Guang Diau*[a, c]*

[a]*Department of Applied Chemistry, National Yang Ming Chiao Tung University, Hsinchu 300093, Taiwan.*

[b]*National Synchrotron Radiation Research Center, Hsinchu 30076, Taiwan.*

[c]*Center for Emergent Functional Matter Science, National Yang Ming Chiao Tung University, Hsinchu 300093, Taiwan.*

Corresponding Author-

E-mail: diau@nycu.edu.tw (Prof. Eric Wei-Guang Diau)

1. Experimental Procedures

For comparative study, hydrothermal syntheses of ZnS samples for different Zn:S precursor ratio was done under the same synthesis conditions. The ZnS was prepared by hydrothermal method. By keeping fix molar concentration of Zn precursor, we varied concentration of S source. The synthesis was done in 120 mL Teflon lined SS autoclave at 180 °C for 12h. We observed that with increase in S concentration during reaction time, the performance of ZnS goes on increasing. The optimized sample for S variation has the Zn:S precursor ratio 1:32 (denoted as ZS0) which produce H_2 yield of 2.6 mmol g^{-1} h^{-1}. The higher concentration of S than this sample will not dissolve in DI water completely meaning that it reaches saturation. The prolonged heating for 12 h at temperature 180° C has maintained high crystallinity of the photocatalysts while the shape anisotropy of the NDs was driven by the presence of acetate and citrate ions. The trigonal planar acetate ions contributed directional growth of these nanocrystals by their alignment along (200) facet of zinc blend structure.[1] Initially, shape and nanoparticle size of ZnS were optimized by increasing the molar concentration of S precursor, where high H_2 evolution was observed for molar ratio of Zn:S to be 1:32. The sample prepared in the absence of tri-sodium citrate (NaCt) is abbreviated as ZS0. Afterwards, for the same Zn:S molar ratio ZnS (ZS), Al-doped ZnS (AZS) and AZS with high Al-doping (AZS*) were synthesized in the presence of NaCt. Figure S1 shows SEM images of these representative samples which reveal particles size variation obtained for different synthetic conditions.

As the S precursor amount increased, the ZnS particle size decreased from the micro to the nanometer scale. The higher S concentration was observed to be beneficial for decreasing the sizes of nanoparticles and hence increasing the active surface area. The Al-doping further decreases the average particle size. The precursor concentration of the dopant Al was optimized by synthesis of AZS at varied molar ratios of Zn:Al. For 1:1 molar ratio of Zn:Al, the 2.2% Al-doping was observed without secondary phase or oxygen (O) species.

However, for increased Al precursor amount (Zn:Al = 1:1.5), this nanostructure disappeared with increased O peak (EDS in Figure S2) and bigger microparticles were formed. For AZS prepared at higher Al^{3+} amount (AZS*), it contains an intense O peak situated at 0.52 keV along with excessive Al atomic percentage (~59%) indicating of secondary species. ZS0 has the particle size of 250 nm (Figure S3a). NaCt-assisted ZS exhibited a similar ND morphology but with a smaller size (135 nm, Figure S3b). Hence, we studied H_2 evolution of this sample and then proceed for the doping in ZnS for the enhancement in H_2 evolution. It was observed that with increase in S precursor amount, H_2 evolution also increases significantly. Therefore, with this Zn:S synthesis conditions, other ZnS samples with optimized tri-sodium citrate (NaCt) concentration (stabilizing agent) and also with Al- doping.

As NaCt can act as both reducing and coordinating agent to avoid the formation of secondary oxide phases in aqueous synthesis at elevated temperature, we introduced NaCt in hydrothermal synthesis of ZnS and Al-doped ZnS. By keeping the same optimized synthesis parameters of ZS0, 10 mmol trisodium citrate dihydrate was dissolved in synthesis mixture of ZS0 and then transferred final mixture to teflon lined autoclave to obtain NaCt mediated ZnS (denoted as ZS). The NaCt concentration was previously optimized for better H_2 yield and used this for Al-doped sample. The Al-doped ZnS (denoted as AZS) was prepared by adding 5 mmol $AlCl_3$ (anhydrous) solution into synthesis parameters of ZS. Since anhydrous $AlCl_3$ is highly oxidative and cause rapid fume formation in water, its aqueous solution was prepared in fumehood by taking proper precautions.

Synthesis of Pt Single atom (SA) decorated ZnS MDs and NDs

The Pt SA sites were deposited on these catalysts by photodeposition method. In particular, 4 μL of H_2PtCl_6 aqueous solution (50mg mL^{-1}) was rapidly injected to 2.5 mg catalysts dispersed in 10% aqueous solution of triethanolamine, TEOA (50 mL) under fast stirring. The mixture was then stirred under dark for 5 min and then transferred to two neck quartz vacuum reactor. The reactor was degassed by using vacuum pump and was purged by ultra-high pure (UHP) Ar gas through rubber sieves by using Ar filled syringe balloon. This step was repeated several times to ensure high inert atmosphere inside the reactor. Finally, after purging Ar in reactor at 1 atm pressure, the system was kept under solar light for 1h. The initial milky white color of the solution mixture changes to different shades of grey depending upon initial weight percentage of Pt solution injected into system. The different amount of Pt solution was used for photodeposition of Pt SAs to check actual loading of Pt on AZS surface. Since ZnS based photocatalyst has wide bandgap in UV region and hence the photodeposition of Pt was found less than actual Pt weight percent solution consumed for SA decoration.

2. Photocatalytic hydrogen evolution

The performance of catalysts was studied by using 380 mL two-neck quartz top-window vacuum reactor. After Pt SA decoration on surface, the sample was collected by centrifugation and the unreacted solvent mixture was discarded. The Pt-coated samples was then cleaned by ethanol, collected by centrifugation and dried in vacuum oven for further characterizations. A 2.5 mg of Pt coated catalyst was dispersed in 50mL of 10% TEOA in DI water. The reactor was degassed and purged by UHP Ar many times until 1 atm reactor pressure has reached. The reactor system was kept under Xenon lamp (500W) with AM1.5G filter for simulated sunlight spectrum and its power intensity was set to one sun by using optical power meter. After a fixed interval of time, the H_2 yield was monitored by injecting 100 μL of gaseous products from the reactor into fused-silica capillary column (column dimensions: length- 30 m, diameter- 0.53 mm) of gas chromatograph (GC, Thermo Trace GC Ultra). The gaseous product yield was measured by using thermally conductive detector (TCD). The reference gas used was UHP Ar with constant inlet flow rate 1 mL min^{-1} throughout the measurements. The front inlet temperature was 200 °C with oven temperature 70 °C and TCD detector was maintained at 300 °C.

3. Characterizations

Spherical aberration-corrected scanning transmission microscopy (JEOL ARM 200F, Cs-corrected STEM) was used for determination of nanostructure morphology and atomic arrangement in single nanoparticle. The obtained STEM micrographs were calibrated and lattice planes were determined by measuring interplanar spacings (software- Gatan DigitalMicrograph). A scanning electron microscope (SEM, JEOL JSM-7401F SEM) and Energy Dispersive Spectroscopy (EDS, detector- Oxford Instruments) were used to monitor particle size distribution and quantitative analysis of elemental distribution in prepared catalysts. The XRD patterns of powder samples were obtained using a Bruker AXS D8 advance X-ray diffractometer (Cu Kα irradiation, $\lambda = 154.18$ pm). The Rietveld refinement for lattice constants was carried out using Fullprof program. Absorption spectra were calculated from diffused reflectance spectra obtained from the JASCO V-780 spectrophotometer with integration sphere accessory. The powder samples were analyzed using X-ray photoelectron spectroscopy (XPS) and ultraviolet photoelectron spectroscopy (UPS; Thermo Fisher Scientific ESCALAB Xi+) to determine their chemical state, BE shifts, Fermi level and VB position. The steady-state photoluminescence spectra were obtained using a laboratory-built PL setup with lock-in amplifier to improve S/N ratio. The 150 W Xenon-Arc lamp light source was used as excitation source with provision of tuning slit width and excitation wavelengths from 300 to 380 nm were set via a monochromator (microHR, Horiba) with a 1200 groove/mm grating and blazing at 330 nm. The emissions were recorded in direction perpendicular to the excitation. For present photocatalysts, emission monochromator's entry slit was adjusted to 1200 groove/mm with 600 nm blaze. The PL emissions were recorded by emission monochromator (TRIAX 320, Horiba). A 480 nm long-pass color glass filter before the emission monochromator entry slit blocked out excitation light. A PicoQuant S3 FluoTime 200 time-correlated single-photon-counting (TCSPC) Spectrometer was used to measure the TRPL lifetimes of ZS and AZS. A 375 nm pulse laser (PicoQuant, LDH-P-C 375) was used for the photoexcitation. To estimate average lifetime, PL decay profiles were fitted using IRF convoluted exponential fits and average lifetime of photoprompted electrons were estimated.

At relatively lower synthesis temperature (180 °C), low doping of Al was done which was confirmed from the thorough investigation of different elemental analysis techniques such as EDAX (Oxford Instruments detector), XPS etc.

The elemental stoichiometry and presence of other impurities in samples was investigated by using EDAX spectra (Figure S2). The higher Al precursor was responsible for excess amount of Al (~59 %) in final product and also oxygen peak was immerged in EDAX spectrum indicates formation of other secondary phases (sample AZS*). Moreover, AZS* has provided very less H_2 yield for HER as compared to other optimized samples. The elemental proportion of different elements in AZS was more precisely obtained from EDAX mapping in Cs-corrected STEM Analysis (JEOL, ARM200F).

4. AQY Calculations

For single photocatalyst system, The AQY was calculated by using following equation:

$$\mathrm{AQY}(\%) = \frac{no.\, of\ reacted\ electrons}{no.\, of\ incident\ photons} \times 100\%$$

Since, two electrons are utilized for formation of single H_2 molecule, AQY will be calculated from knowing H_2 yield as:

$$= \frac{no.\, of\ H_2\, molecules\ generated \times 2}{no.\, of\ incident\ photons} \times 100\%$$

For example, AQY for Pt-AZS under irradiation of 345 nm (WB40) is calculated as follows,

$$\mathrm{AQY} = \frac{no.\, of\ H_2\, molecules\ generated \times 2}{no.\, of\ incident\ photons} \times 100\%$$

$$= \frac{N_A \times Y \times 2}{N} \times 100\%$$

$$= \frac{N_A \times Y \times 2}{{E\lambda}/{hc}} \times 100\% \qquad (1)$$

where, N_A is Avogadro's no. = 6.022×10^{23}, Y is H_2 yield in mol = 20.32×10^{-6} for a fixed hour, N is the total no. of incident photons for a fixed hour, E is the incident light density for the same hours, λ is incident wavelength, *h* is Planck constant, and c is speed of light then,

$$\mathrm{N} = \frac{E\lambda}{hc} = \frac{1.43 \times 10^{-3} \times 345 \times 10^{-9} \times 8 \times 3600}{6.626 \times 10^{-34} \times 3 \times 10^{8}} = 7.18 \times 10^{19}$$

Then eq (1) becomes,

$$\mathrm{AQY} = \frac{6.022 \times 10^{23} \times 2.023 \times 10^{-5}}{7.18 \times 10^{19}} \times 100\ \% = 34.11\ \%.$$

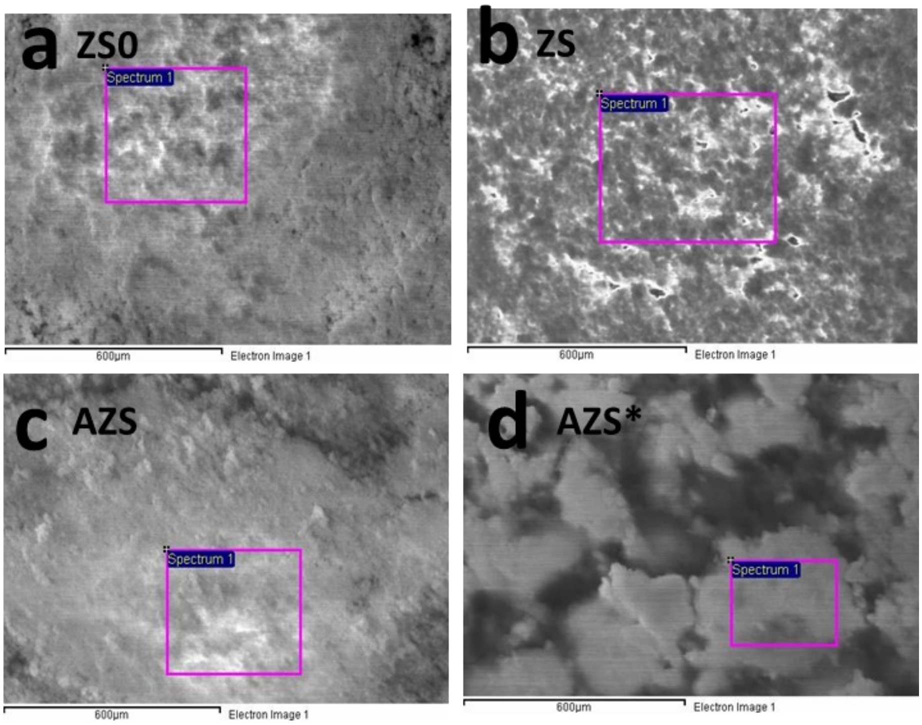

Figure S1. SEM images of a) ZnS samples prepared without NaCt (ZS0), b) ZnS samples prepared with NaCt (ZS), c) AlSA-ZnS (AZS), and d) AZS with high Al-doping concentration (AZS*).

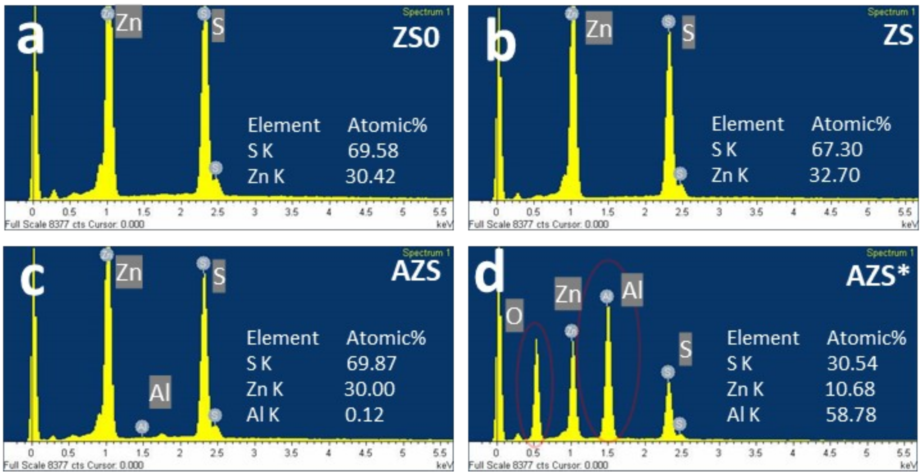

a ZS0

Element	Atomic%
S K	69.58
Zn K	30.42

b ZS

Element	Atomic%
S K	67.30
Zn K	32.70

c AZS

Element	Atomic%
S K	69.87
Zn K	30.00
Al K	0.12

d AZS*

Element	Atomic%
S K	30.54
Zn K	10.68
Al K	58.78

Figure S2. EDAX spectra of a) ZS0, b) ZS, c) AZS and d) AZS*.

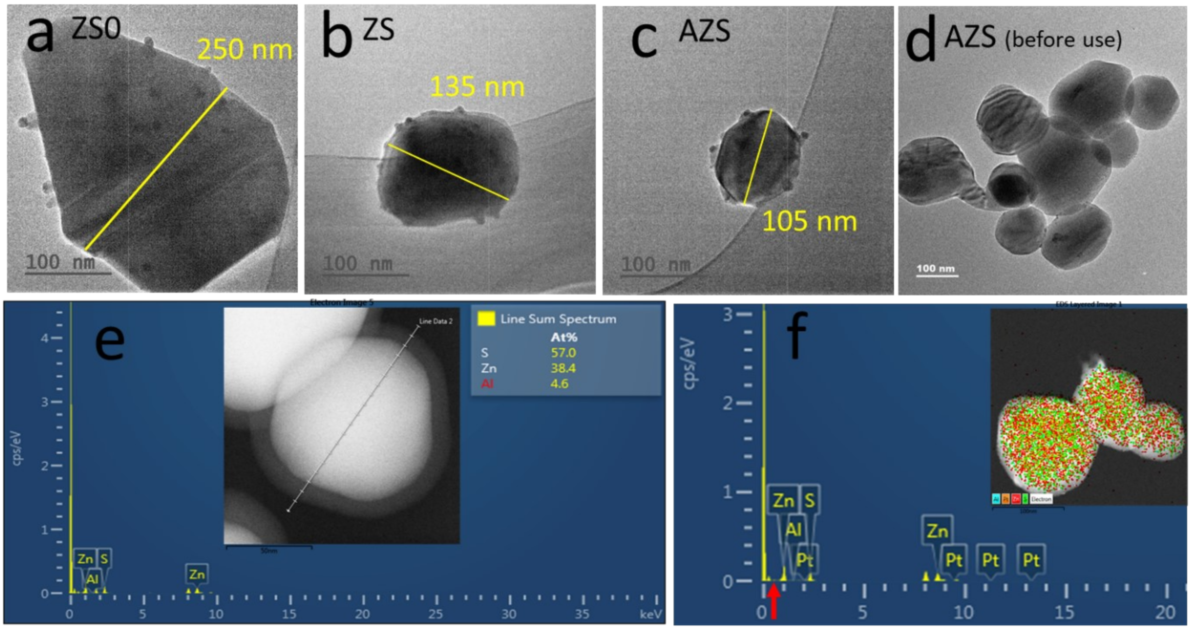

Figure S3. TEM images of (a) ZS0, (b) ZS and (c) prepared using bare Zn, S precursors. (b) with additional NaCt (ZS). (c) AlSA-ZnS ZnS using NaCt (AZS). (d) TEM image of AZS before photocatalytic study; average diameter ~110 nm. (e) Line scan EDS spectrum of AZS and (f) EDS elemental Spectrum of Pt-AZS in TEM mapping mode. The red arrow shows BE Kα line position of O (~0.52 keV), inset shows elemental distribution in Pt-AZS.

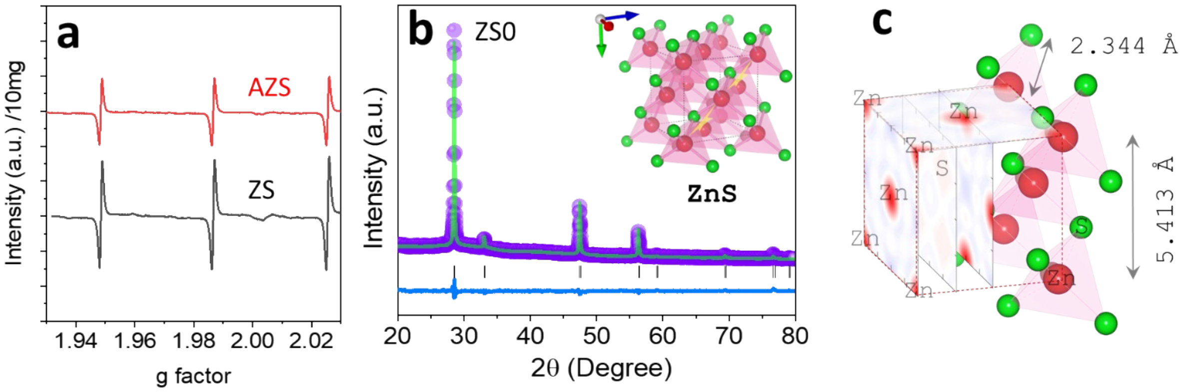

Figure S4. (a) EPR spectra of ZS and AZS measured under the same mass and test parameters. (b) Rietveld refinement of XRD data of ZS0. The inset shows EDMs at x=0 along the [100] axis. (c) the distribution of electron densities in unit cells of ZS0.

The XPS peak positions were accurately determined by calibration of Au $4f_{7/2}$ (84.0 eV) peak position in Au XPS spectrum. In AZS, the XPS peaks corresponding to Zn 2p appear at higher binding energies with minor up shifts of 0.3 eV compared to those of the ZS sample. Zn $2p_{3/2}$ and $2p_{1/2}$ peaks of AZS are located at 1021.3 eV and 1044.3 eV, respectively. The increase in binding energies imply partial increase in valence state of Zn^{2+} by charge transfer to dopant Al and this contribution can be determined by using maximum likelihood fitting with fixed broadening (FWHM) to Zn $2p_{3/2}$ and $2p_{1/2}$ peaks of both ZS and AZS, respectively. The additional contribution fitted by two new satellite peaks near Zn $2p_{3/2}$ and $2p_{1/2}$ at higher binding energies (1022.4 eV and 1045.4 eV, respectively) corresponds to charge transfer by the hybridization of partially occupied Al 3p and Zn 3d orbitals. This modified charge distribution can be beneficial for suppressing charge recombination.

The survey spectra of ZS0, ZS, and AZS reveal the coexistence of Zn and S with estimated atomic percentage shown in the Figure S5. As the XPS was obtained by using Al K-α source gun with electron binding energy 1487 eV, the low energy Al 2p peak at 74 eV has weak signal. This is due to the low photoionization cross section of Al 2p peak for such a high energy gun source. As a result, by comparing survey and individual elemental XPS spectra, a less intense Al 2p peak was observed for high Al atomic concentration AZS* (Figure S6). For constant energy Al K-α source, the peak intensities are sensitive to photoionization cross section of the elements and bigger step size of 0.1 eV is inefficient to detect low concentration of Al in AZS (here 2.2% Al was obtained from EDS mapping of TEM images). Figure S7 gives XPS spectra of ZS and AZS in which for pristine ZS shown in Figure S7a, the XPS peaks contain characteristic doublets of Zn $2p_{3/2}$ and $2p_{1/2}$ located at 1021.0 eV and 1044.0 eV, respectively.

For ZS shown in Figure S7b, after deconvoluting of the S 2p XPS peaks, binding energies 161.3 eV and 162.4 eV corresponding to $2p_{3/2}$ and $2p_{1/2}$, respectively, were obtained.

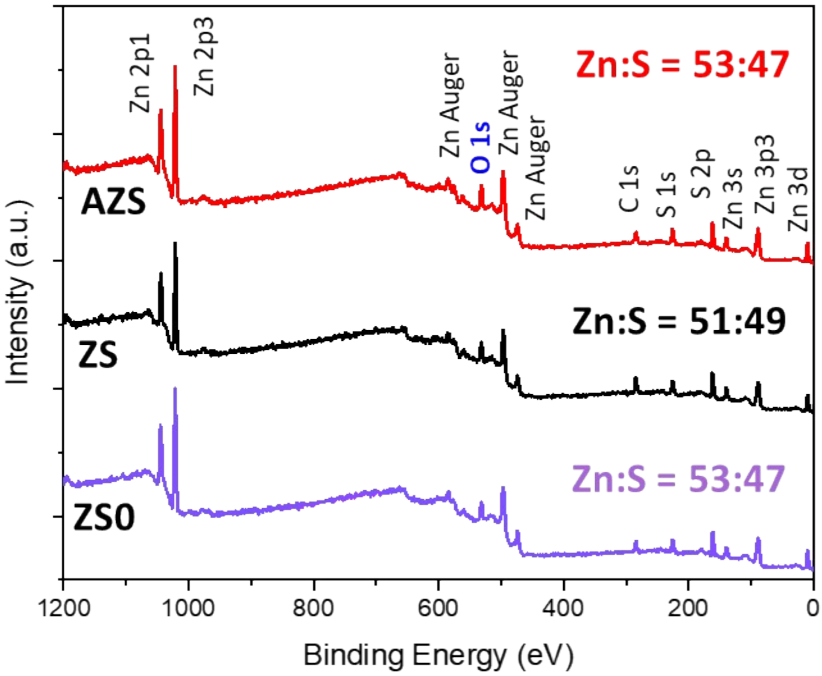

Figure S5. XPS survey spectra of ZS0, ZS and AZS obtained using Al K-α source gun with electron binding energy of 1497 eV.

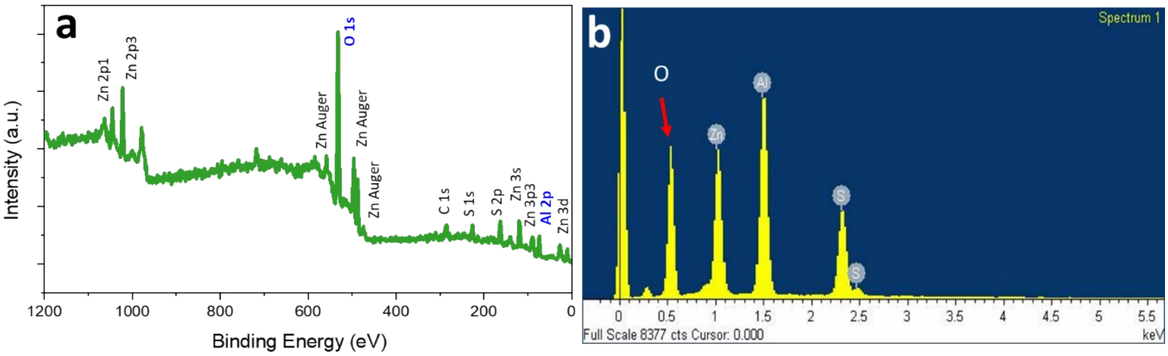

Figure S6. (a) XPS survey spectra of AZS* showing minor Al 2p peak at 73.2 eV, (b) corresponding EDS spectrum showing high concentrations of Al and O.

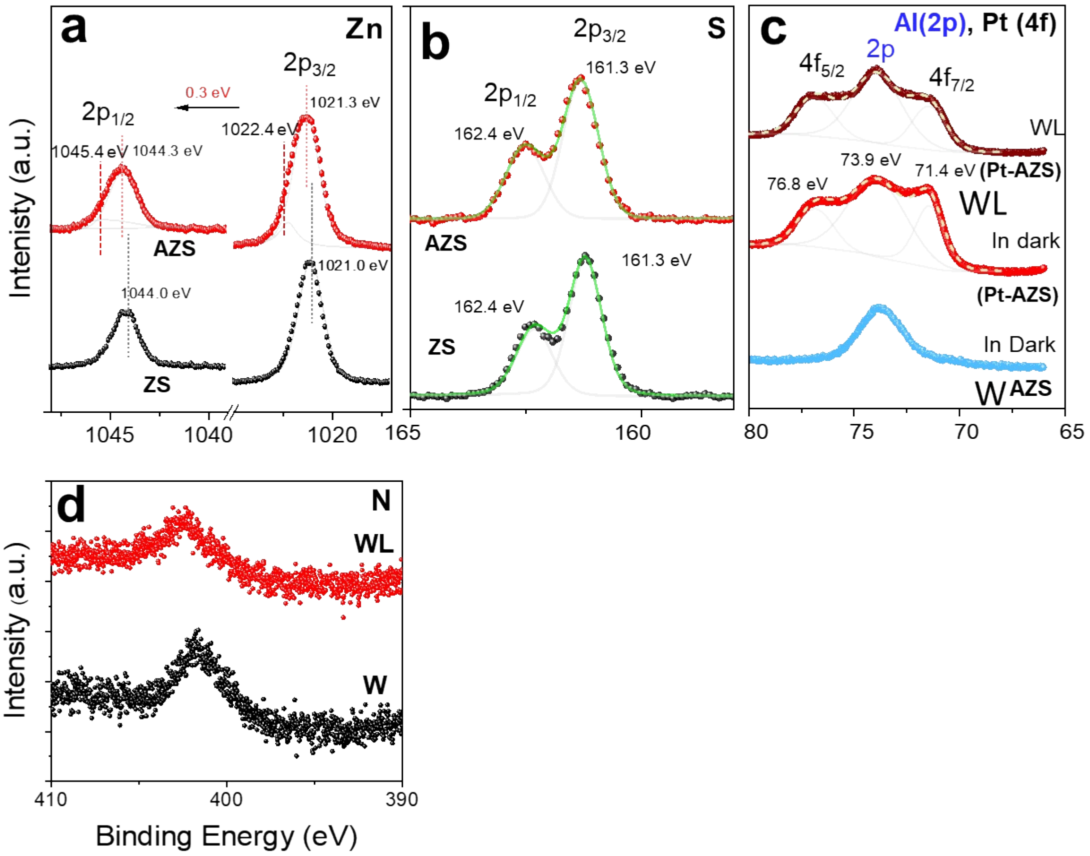

Figure S7. The XPS spectra for a) Zn 2p, b) S 2p, c) Pt 4f and Al 2p core levels of ZS, AZS, Pt-AZS samples in vacuum without light irradiation. (d) *in situ* XPS spectra for N 1s in the presence of water vapors and under light irradiation on TEOA adsorbed Pt-AZS film.

For in situ XPS, the Pt-AZS coated ITO substrate (modified by TEOA adsorption) was vertically suspended in the XPS chamber and maintained under low pressure with controlled water vapor environment. In Pt-AZS, a higher work function (Φ) of Pt (5.3 eV) developed Mott-Schottky junction by aligning with the Fermi level of AZS. As shown in Figure 4a and 4b, for Pt-AZS, the binding energies of Zn 2p and S 2p under dark conditions (initial measurement W) were observed at similar positions as those of AZS (Figures S7a and S7b). Given the constraints of a substrate dimension (15×15 mm^2) and a smaller spot size of light probe (<10 mm), it is possible to accurately track the peak shifts in the Zn and S 2p core levels by enhancing the charge transfer from AZS to Pt SA sites. Additionally, for effectively decrease of electron-hole recombination and chemical stability under full light irradiation, TEOA (hole scavenger) was also introduced.

For in-depth study of microscopic shape and porosity (or rigidity) of AZS, the N_2 adsorption–desorption isotherm measurement was performed to determine surface area and pore diameter distribution of AZS. As shown in Figure S8, the anisotropic shape of AZS grooved virtual pores among themselves with bigger diameter but least volume. The lower specific surface area of AZS (1.69 m^2 g^{-1}) also depicts compact structure owing to its uninterrupted crystal growth which can improve photoexcitation of the catalyst by wider S-rich (200) facet exposing to light, thereby would boost up the H_2 evolution rate. The N_2 adsorption-desorption isotherm linear plot and pore size distribution shown in Figure S8a and S8b exhibit type III isotherm with H3 hysteresis, indicating plate-like rigid nanostructure of AZS. The Barrett-Joyner-Halenda (BJH) desorption cumulative pore size curve revealed the low average pore volume of 0.0049 cm^3 g^{-1} with calculated BET pore diameter of 232.9 nm which reflects highly compact growth of prepared AZS NDs.

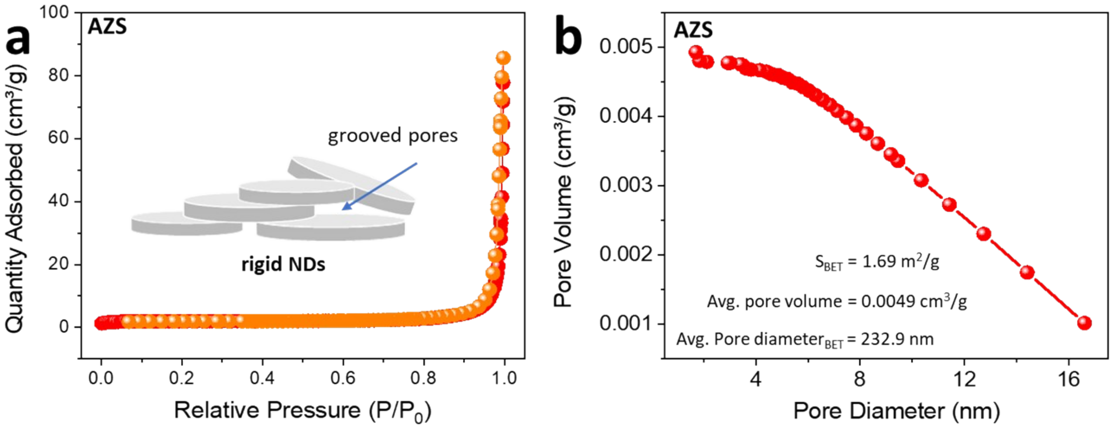

Figure S8. a) The N_2 adsorption-desorption isotherm and b) pore diameter distribution of AZS.

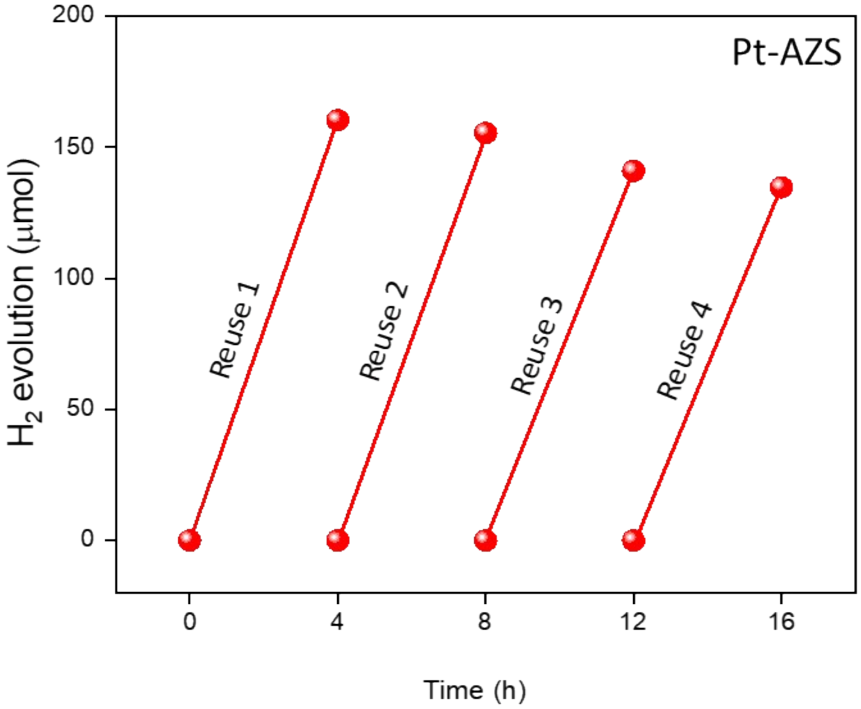

Figure S9. The cyclic H_2 evolution performance of Pt-AZS for 4h under AM1.5G irradiation.

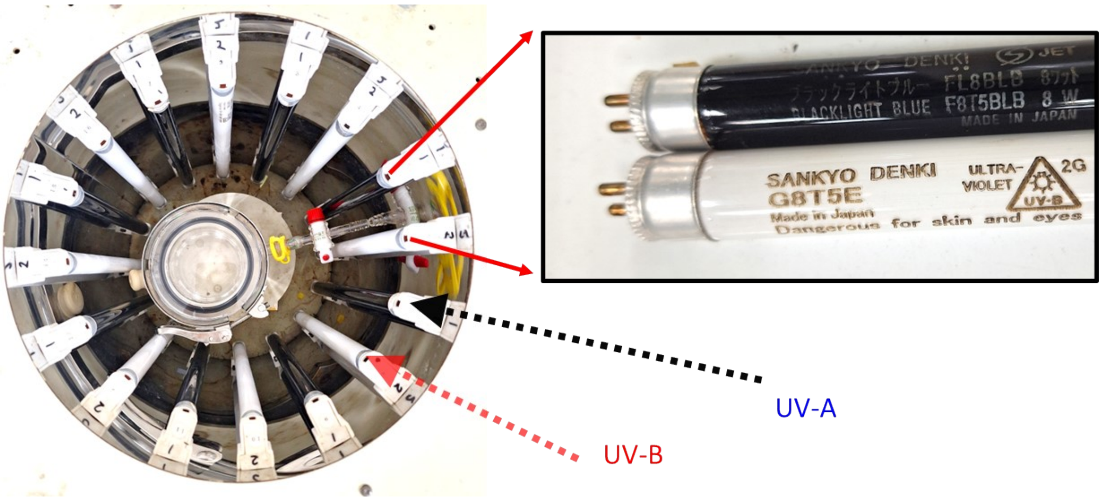

Figure S10. The two channel UV-reactor with provision of UV-A (black tube-lights), UV-B (white tube-lights) spectra. The 8W UV-A (F8T5BLB) source has longer UV wavelength while 8W UV-B (G8T5E) source has shorter UV wavelength.

Eventually, Pt-AZS was deposited on glass substrate (4×4 cm^2) by drop-casting of methanol dispersed solution containing 10 mg Pt-AZS. The resultant thin film was used for photocatalytic H_2 evolution where the air from reactor was evacuated. After light irradiation, the H_2 bubbles came out quickly above the film surface (Figure S11a and supplementary movie 1) with considerably high H_2 generation rate of 20.887 mmol $h^{-1}m^{-2}$ (0.468 L $h^{-1}m^{-2}$) under AM1.5G solar irradiation. This HER performance is greater than the previously reported C_3N_4 film (0.19 L $h^{-1}m^{-2}$) and Pt_{SS}-MOF (0.398 L $h^{-1}m^{-2}$). [1, 2]

By continuous utilization of TEOA for holes annihilation and Cl^- release by Pt photodeposition, the transparency of the solution with yellowish tint (Figure S11d). However, structural stability of Pt-AZS was maintained even after 48h AM1.5G solar light driven H_2 evolution experiment (XRD patterns in Figure S12). Also, no adverse effect on Pt-AZS morphology was seen after 48h light irradiation (Figure S13).

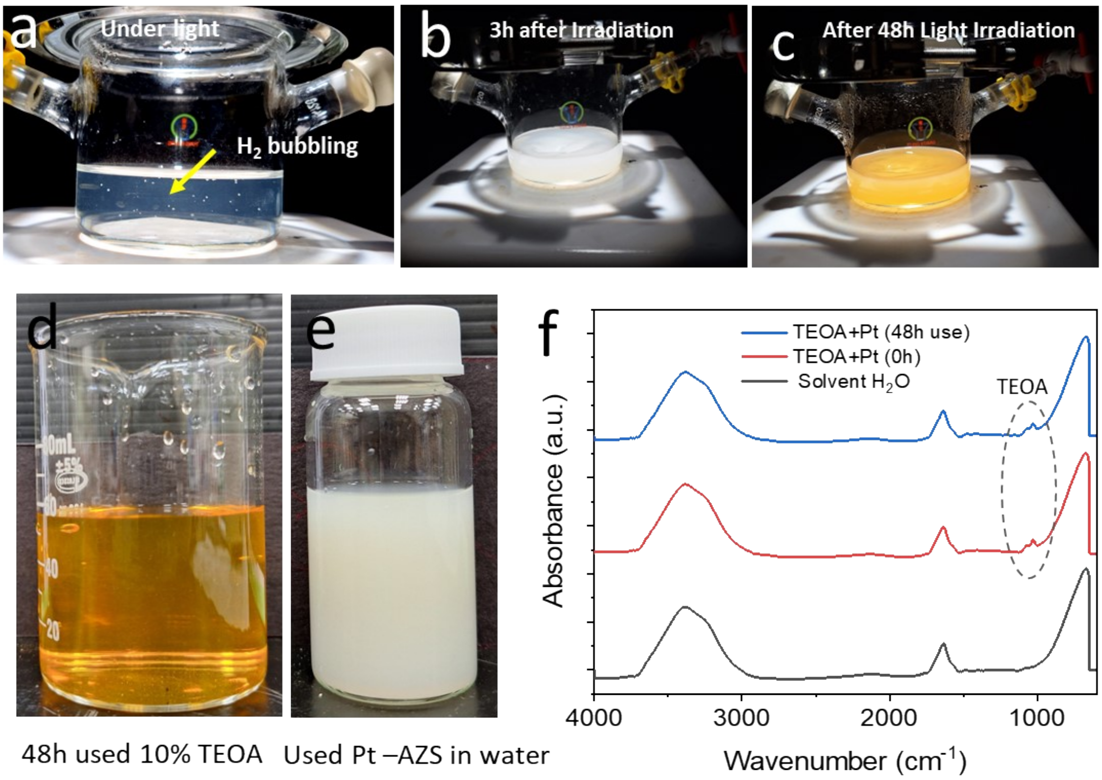

48h used 10% TEOA

Used Pt –AZS in water

Figure S11. The Pt-AZS in 10 vol % aqueous TEOA (a) H_2 bubbling (b) after 3h light irradiation c) after 48 h of light treatment. (d) formation resulted in yellowish tint to solvent due to Cl- release after Pt deposition. (e) extracted Pt-ZnS and redispersion in water showed phase stability of Pt-AZS. (f) ATR spectra of fresh and 48h used TEOA+Pt sol^n.

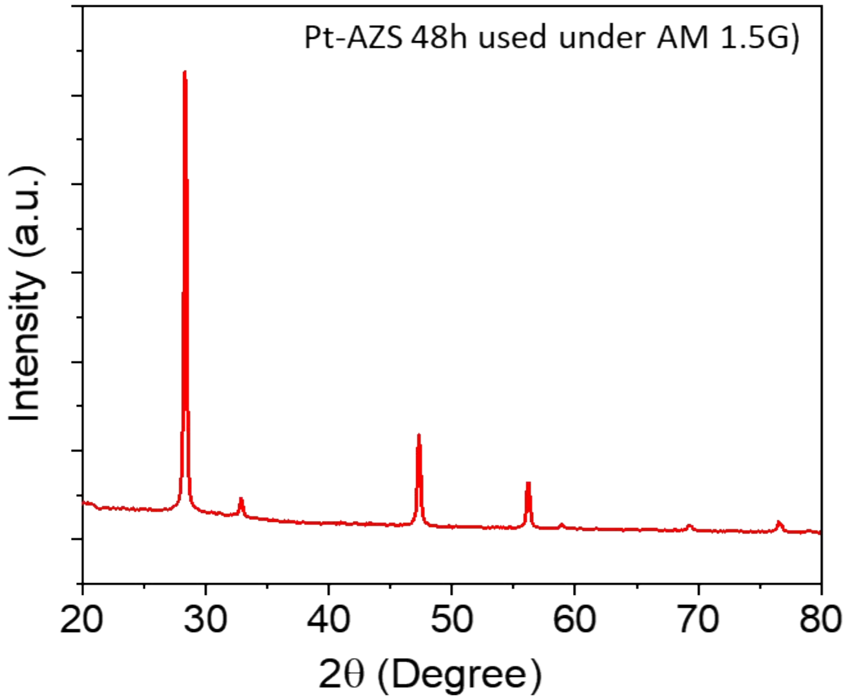

Figure S12. XRD patterns of Pt-AZS under AM1.5G irradiation for 48 h.

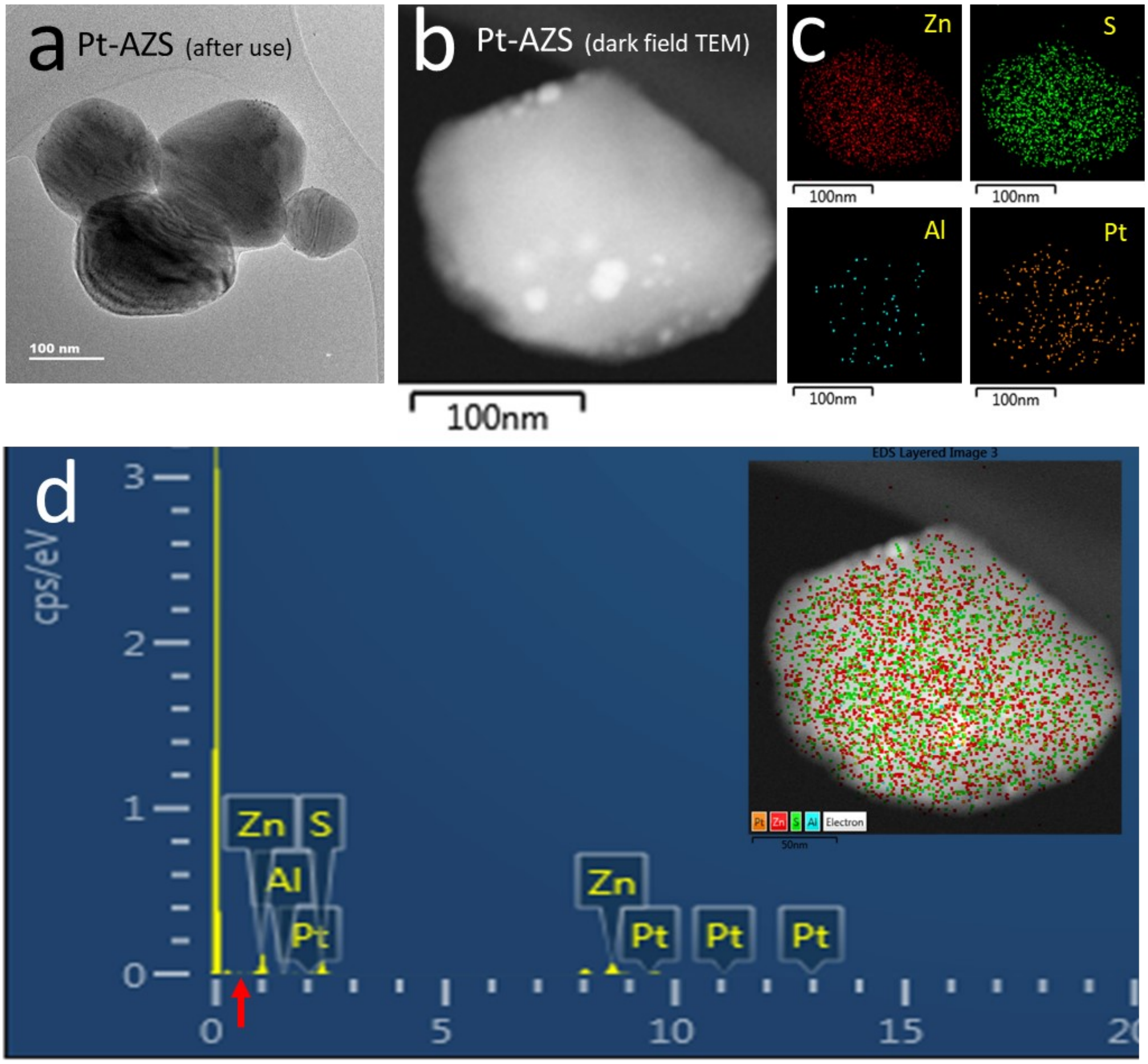

Figure S13. (a)TEM image of 48h used Pt-AZS. (b) dark field TEM and (c) EDS mapping of Pt-AZS after 48h light irradiation under H_2 evolution reaction and (d) EDS elemental Spectrum of Pt-AZS after 48h use. The red arrow shows BE Kα line position of O (~0.52 keV), inset shows elemental distribution in Pt-AZS after 48h use for photocatalytic H_2 evolution.

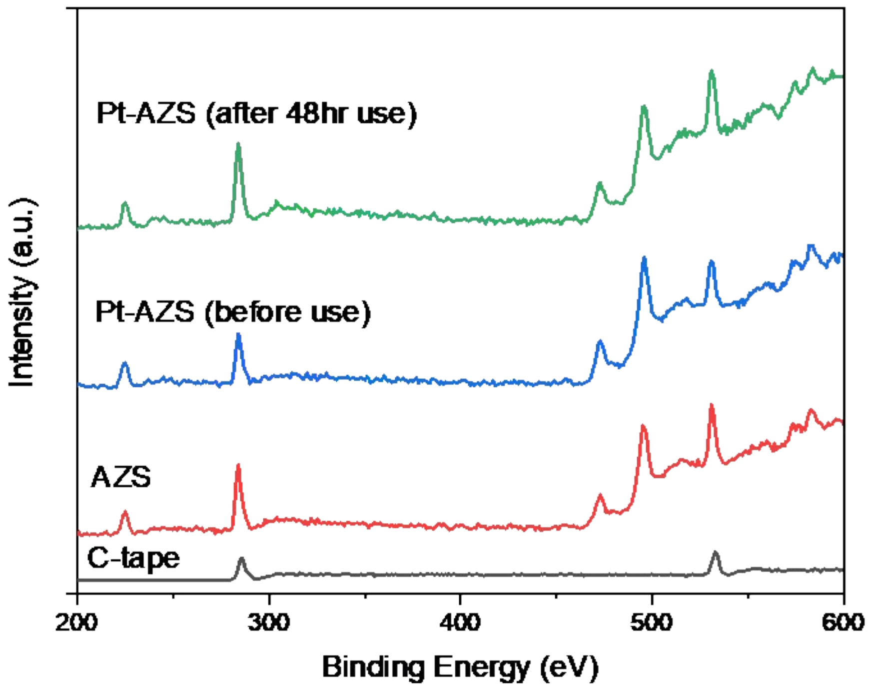

Figure S14. XPS survey spectra of C-tape, AZS, Pt-AZS (before use for H_2 evolution) and Pt-AZS (before use for H_2 evolution) showing the regions of C 1s and O 1s core levels.

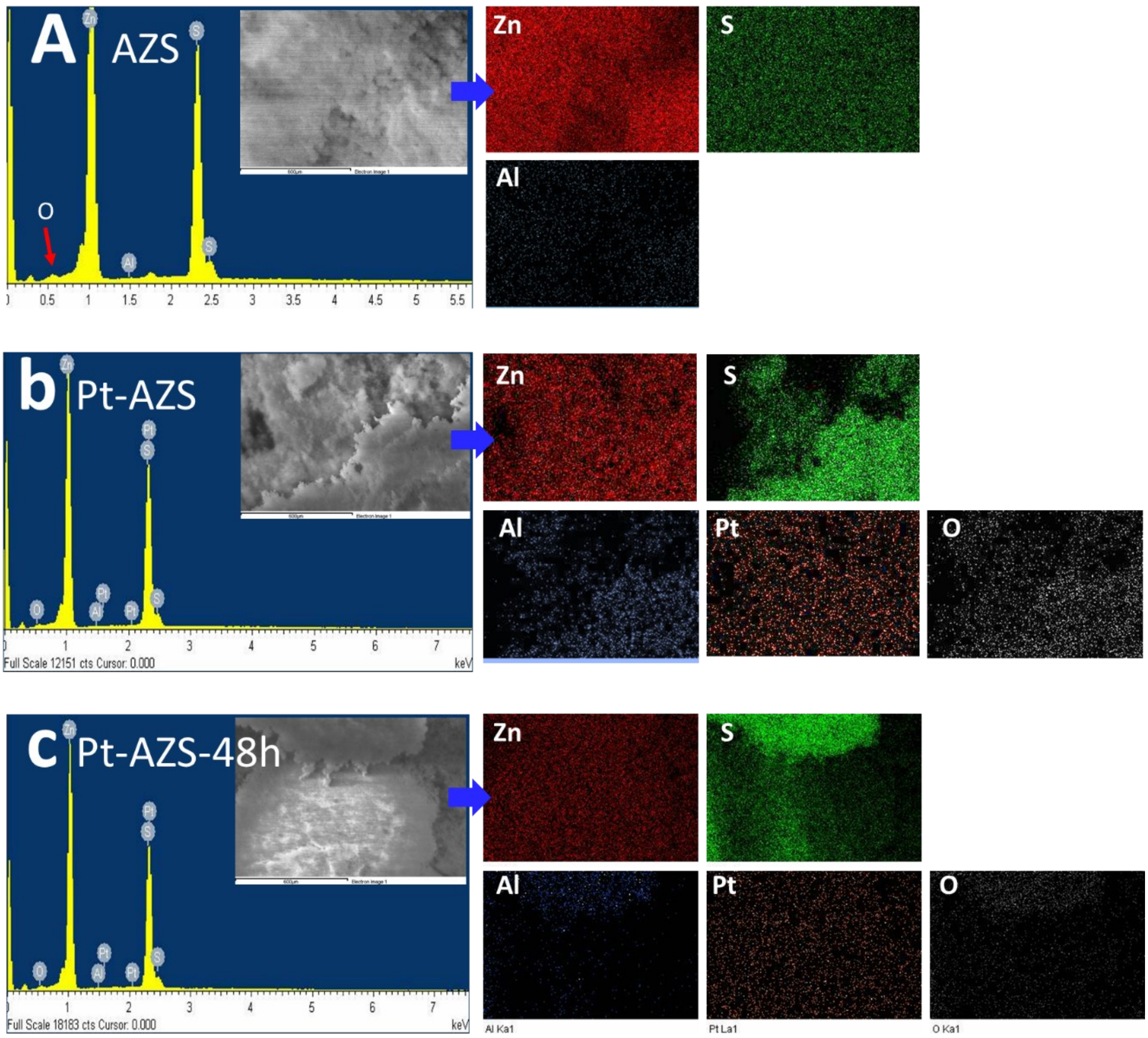

Figure S15. EDS spectra of (a) AZS, (b) Pt-AZS (before use for H_2 evolution) and (c) Pt-AZS (before use for H_2 evolution) with respective elemental mappings.

The UV-Vis diffused reflectance spectroscopy (DRS) method was used to analyze the optical absorption characteristics; the band-gap (E_g) is estimated from the equation, $(F(R)h\nu)^2 = A(h\nu - E_g)$, where the absorption coefficient $F(R) = \frac{(1-R)^2}{2R}100\%$ is Kubelka-Munk function, h is Plank constant and ν is frequency of the incident photons. Both ZS and AZS exhibit considerable absorption in the UV region, with AZS displaying a small and broad band in the visible region from 400 to 600 nm (Figure S16a). The bandgap energies of both samples are found to be the same (inset of Figure S14a, E_g = 3.66 eV). However, the increased light absorption in AZS promotes the production of more photocarriers, which in turn improves the photocatalytic activity.[3] The weak visible absorption has been attributed to the defect states caused by the introduction of Al dopant into the ZnS lattice, indicating disorder in the lattice that has been previously explained in the XRD analysis. During photocatalysis, some of the electrons generated after light irradiation are utilized in a reduction reaction, while others recombine with holes. The AQY measurements confirmed that the UV absorption contributed most HER yields while the weak below band gap absorption provided very little contribution on the HER yields.

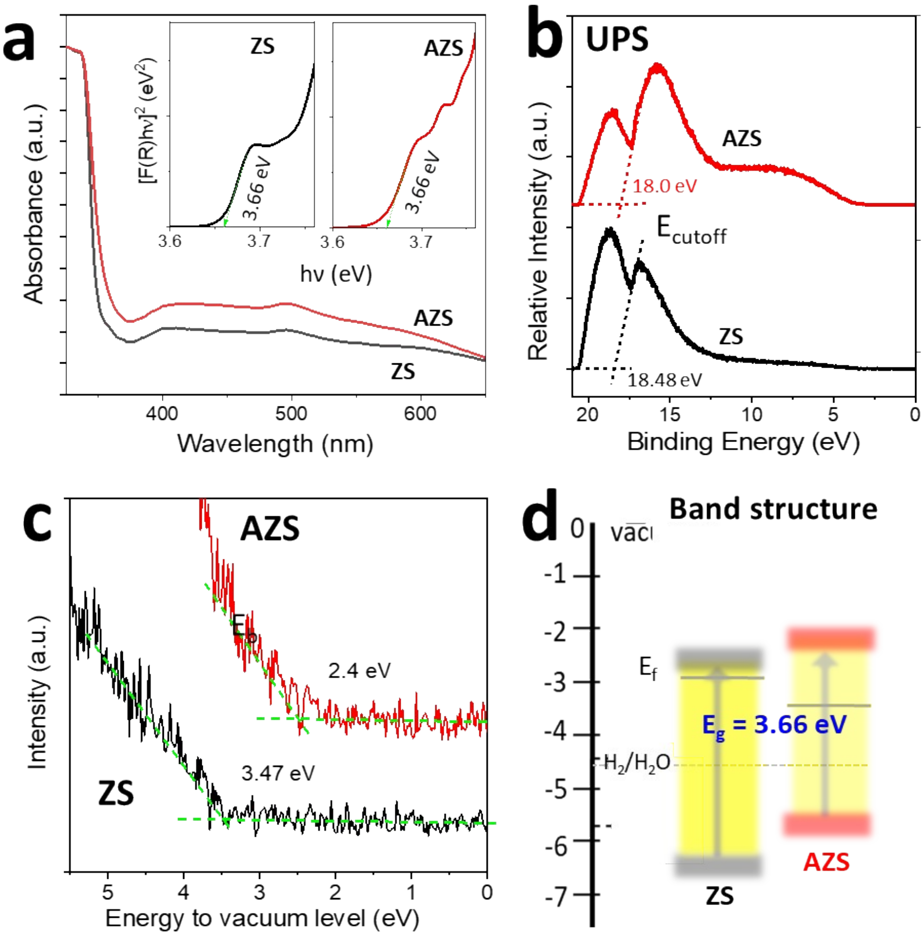

Figure S16. a) Normalized UV-vis absorption spectra of ZS and AZS. The inset shows bandgaps determination from Kubelka-Munk function; b) UPS spectra of ZS and AZS with cutoff energies and c) binding (Eb) energies; d) The energy band structure diagrams of ZS and AZS.

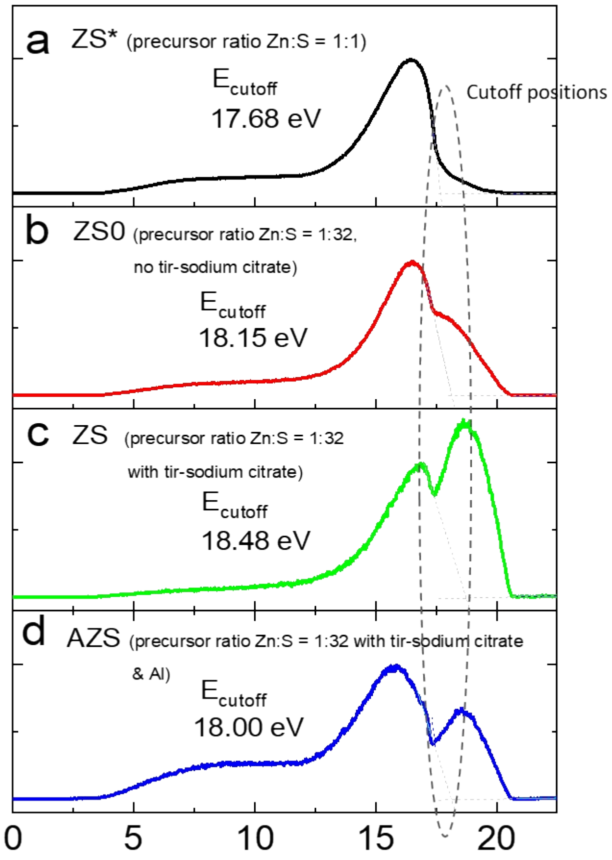

Figure S17. UPS Spectra of ZnS and AlSA-ZnS prepared at different synthesis conditions.

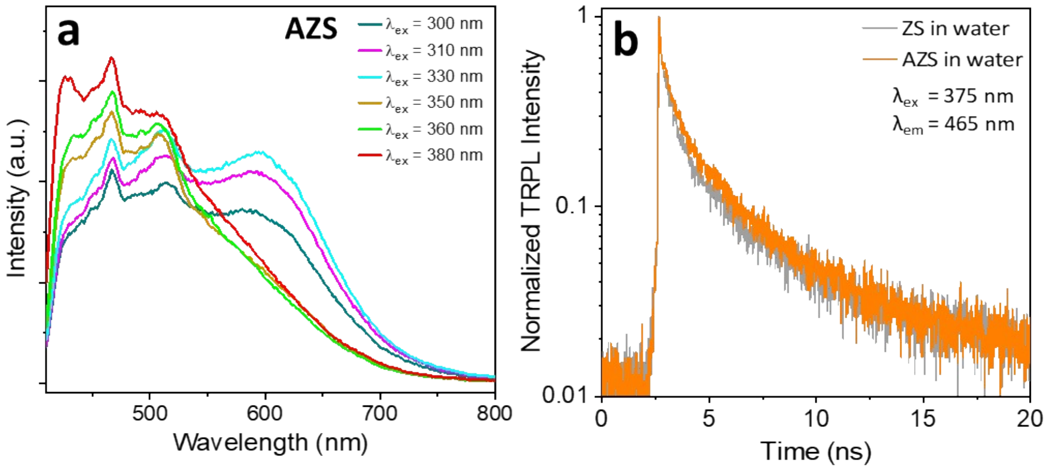

Figure S18. (a) Steady-state photoluminescence (PL) emission spectra of aqueous dispersion of ZS recorded at different excitation wavelengths; (b) TRPL decay profiles of aqueous suspensions samples.

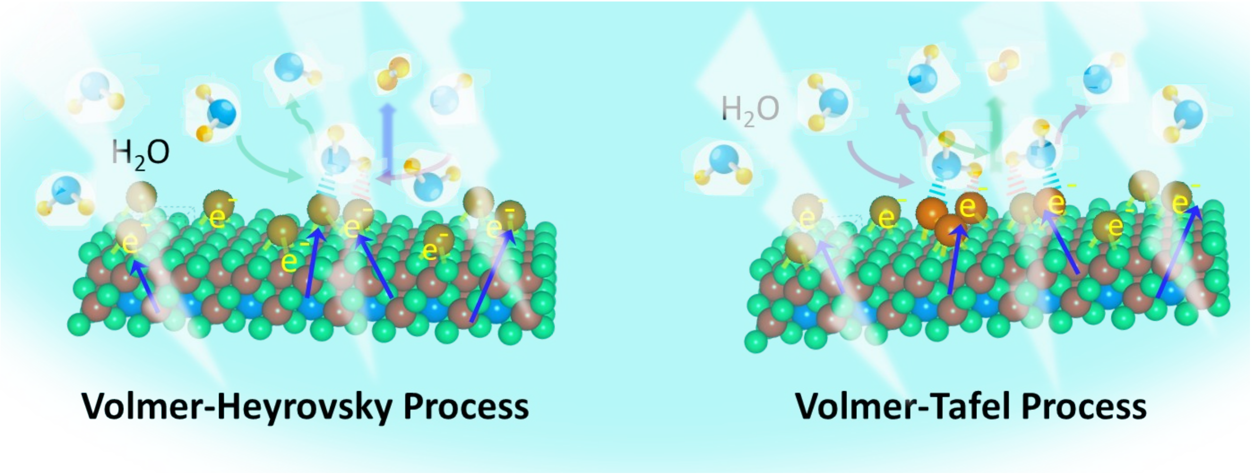

Figure S19. Schematic of H_2 evolution at Pt SA sites by Volmer-Heyrovsky or Volmer-Tafel mechanism.

The initial Pt SA photodeposition is done by utilizing these photogenerated electrons for reduction of $[PtCl_6]^{2-}$ and is shown by equation 1:

$$[PtCl_6]^{2-} + 4e^- \rightarrow Pt + 6Cl^- \qquad (1)$$

Since, the alkaline aqeous TEOA system (pH ~10) was used for H_2 evolution. HER involves adsorption and dissociation of water followed by H-O-H bond breaking to generate adsorbed hydrogen atoms (H_{ads}). In alkaline system, due to lower proton counts, an extra energy (photoexcited electrons) is spent for generation of protons. Since the adsorption strength of H on metal sites decreases with increase in its count, the limited no. of H-intermediates (H_{ads}) is adsorbed on Pt SA sites by conforming balance between the H-H electrostatic repulsion and the orbital hybridization of Pt-H.

Thereafter, the photopromted electrons are consumed by H_{ads} to give H_2 by following Volmer-Heyrovsky or Volmer-Tafel mechanism as shown in equation 2-5 and schematically represented in Figure S19:

$$H_2O \rightleftharpoons H^+ + OH^- \qquad (2)$$

Volmer-step-

$$H^+ + OH^- + e^- \rightarrow H_{ads} + OH^- \qquad (3)$$

Heyrovsky-step-

$$H_{ads} + H_2O + e^- \rightarrow H_2\uparrow + OH^- \qquad (4)$$

or Tafel-step-

$$2H_{ads} \rightarrow H_2\uparrow \qquad (5)$$

Table S1. ICP-MS data of Pt-AZS

Element	**Pt**	**Al**	**Zn**	**S**
Sample	**Concentration**			
Pt-AZS	wt%	wt%	wt%	wt%
	1.635	0.995	62.19	20.98
	At%	At%	At%	At%
	0.602	2.198	59.539	37.661

Table S2. The photon counts and photocatalytic H_2 evolution using different wavelengths.

Wavelength of band pass filter (nm)	**Illuminance** (Lux)	**Area of exposure** cm^2	**Irradiation time** h	**Total no. of photons**	**H_2 yield** μmol
345±20 nm (WB40)	16.73	5.07	8	7.176×10^{19}	20
365±20 nm (WB50)	31.54			9.721×10^{19}	0.28
380±10 nm	226.33			1.462×10^{20}	0.105
400±10 nm	191.86			9.443×10^{19}	0.140
420±10 nm	315.39			1.300×10^{20}	0.07

Table S3. The O level comparison in AZS and Pt-AZS at different conditions

Sample	Condition	Area		C_{Area}/O_{Area}
		C	O	
Carbon tape	conducting	80941	78651	1.067
AZS	as prepared	200424	191480	1.047
Pt-AZS	Pt- photodeposited	161277	154963	1.041
Pt-AZS-48h	H2 evolution study (48h)	252011	249332	1.011
AZS*	High Al, O	42891	268855	0.159

Table S4. Lifetime parameters from tri-exponential fitted TRPL decay curves measured at 460 nm (λ_{em}) after laser excitation of 375 nm (λ_{ex}) for ZS and AZS thin films.

photocatalysts **(powder thin film)**	**τ_1** (ns)	**A_1** (%)	**τ_2** (ns)	**A_2** (%)	**τ_3** (ns)	**A_3** (%)	**τ_{Av}** (ns)	
ZS	0.54	31.57	5.71	47.99	39.34	20.44	2.26	(amplitude weighted)
AZS	0.65	21.25	5.631	33.65	39.93	45.10	2.50	(amplitude weighted)

Table S5. Lifetime parameters from bi-exponential fitted TRPL decay curves measured at 465 nm (λ_{em}) after laser excitation of 375 nm (λ_{ex}) for aqueous suspension of ZS and AZS.

photocatalysts **(aq suspension)**	τ_1 (ns)	A_1 (%)	τ_2 (ns)	A_2 (%)	τ_{Av} (ns)
ZS	0.69	34.28	5.61	65.72	1.63 (amplitude weighted)
AZS	0.90	36.08	5.58	63.92	1.95 (amplitude weighted)

Supporting References

[1] Q. Zuo, T. Liu, C. Chen, Y. Ji, X. Gong, Y. Mai, Y. Zhou, Angewandte Chemie International Edition 2019, 58, 10198.

[2] M. Schröder, K. Kailasam, J. Borgmeyer, M. Neumann, A. Thomas, R. Schomäcker, M. Schwarze, Energy Technology 2015, 3, 1014.

[3] U. P. Gawai, U. P. Deshpande, B. N. Dole, RSC Adv 2017, 7, 12382.